



HAL
open science

Identification of Parameters of Host Cell Vulnerability during Salmonella Infection by Quantitative Image Analysis and Modeling

Jakub Voznica, Christophe Gardella, Ilia Belotserkovsky, Alexandre C Dufour, Jost Enninga, Virginie Stévenin

► **To cite this version:**

Jakub Voznica, Christophe Gardella, Ilia Belotserkovsky, Alexandre C Dufour, Jost Enninga, et al.. Identification of Parameters of Host Cell Vulnerability during Salmonella Infection by Quantitative Image Analysis and Modeling. *Infection and Immunity*, 2017, 86 (1), 10.1128/IAI.00644-17 . pasteur-01899398

HAL Id: pasteur-01899398

<https://pasteur.hal.science/pasteur-01899398>

Submitted on 22 Oct 2018

HAL is a multi-disciplinary open access archive for the deposit and dissemination of scientific research documents, whether they are published or not. The documents may come from teaching and research institutions in France or abroad, or from public or private research centers.

L'archive ouverte pluridisciplinaire **HAL**, est destinée au dépôt et à la diffusion de documents scientifiques de niveau recherche, publiés ou non, émanant des établissements d'enseignement et de recherche français ou étrangers, des laboratoires publics ou privés.

1
2
3
4 Identifying parameters of host cell vulnerability during
5 *Salmonella* infection by quantitative image analysis and
6 modeling
7
8
9

10
11
12 **Jakub Voznica^{1,2,3}, Christophe Gardella^{4,5}, Ilia Belotserkovsky⁶, Alexandre Dufour²,**
13 **Jost Enninga¹, Virginie Stévenin^{1*}**
14
15
16
17

18 ¹Institut Pasteur, Dynamics of Host-Pathogen Interactions Unit, 25 rue du Dr. Roux, 75724
19 Paris, France

20 ²Institut Pasteur, BioImage Analysis Unit, 25 rue du Dr. Roux, 75724 Paris, France

21 ³Ecole Normale Supérieure de Cachan, Université Paris-Saclay, 61 avenue du Président
22 Wilson, 94235 Cachan, France

23 ⁴Laboratoire de Physique Statistique, CNRS, UPMC and Ecole Normale Supérieure, 24, rue
24 Lhomond, 75005 Paris, France

25
26 ⁵Institut de la Vision, INSERM and UPMC, 17 rue Moreau, 75012 Paris, France
27

28 ⁶Institut Pasteur, Molecular Microbial Pathogenesis Unit, 25 rue du Dr. Roux, 75724 Paris,
29 France

30
31
32 *For correspondence:

33 Virginie Stévenin

virginie.stevenin@ens-cachan.fr

34
35 **Key words:**

36 *Salmonella enterica* serovar Typhimurium, cooperative behavior, cell vulnerability, single-cell
37 heterogeneity, mathematical modeling.
38

39 **Running title:**

40 Cell vulnerability during *Salmonella* infection

41 **ABSTRACT**

42

43

44 *Salmonella* targets and enters epithelial cells at permissive entry sites: some cells are more
45 likely to be infected than others. However, the parameters that lead to host cell heterogeneity
46 are not known. Here, we quantitatively characterized host cell “vulnerability” towards
47 *Salmonella* infection based on imaged parameters. We performed successive infections of
48 the same host cell population followed by automated high-throughput microscopy and
49 observed that infected cells have higher probability of being re-infected. Establishing a
50 predictive model we identified two combined origins of host cell vulnerability: the pathogen-
51 induced cellular vulnerability emerging from *Salmonella* uptake and persisting at later stage
52 of the infection, and the host cell-inherent vulnerability. We linked the host cell inherent
53 vulnerability with its morphological attributes such as the local cell crowding, and with host
54 cell cholesterol content. This showed that the probability of *Salmonella* infection success can
55 be forecast from morphological or molecular host cell parameters.

56 INTRODUCTION

57

58 *Salmonella enterica* serovar Typhimurium (*S. Typhimurium*) is a Gram-negative bacterium
59 that causes enteric diseases in many vertebrates after ingestion of contaminated food or
60 water. Salmonellosis is one of the most common causes of food-borne diseases in humans
61 and is considered to be major public health and global economic problem (1). After oral
62 uptake, more than 99% of *S. Typhimurium* are killed in the stomach or in the gut (2). The
63 surviving bacteria reach the distal ileum where they invade non-phagocytic intestinal
64 epithelial cells (3). *In vitro* experiments have shown that *S. Typhimurium* invasion of host
65 cells occurs after a phase of bacterial "Near Surface Swimming" (NSS) on the epithelial
66 layer. The bacteria scan the surface and eventually stop and dock at a "selected" host cell
67 (4), (5). Docking is irreversible (6) and followed by injection of *Salmonella* effectors into the
68 host cell through a Type 3 Secretion System (T3SS), leading to the formation of ruffles that
69 engulf the incoming bacterium (7), (8). Upon internalization *S. Typhimurium* either develops
70 inside a *Salmonella*-Containing Vacuole (SCV) or it ruptures the SCV to escape into the
71 cytoplasm where the pathogen replicates at a high rate, a phenomenon called
72 hyperreplication (HR) (9, 10).

73

74 The mechanism by which *S. Typhimurium* targets specific host cellular sites for its entry
75 remains debated. Santos and colleagues suggested that mitotic cells are selected due to
76 increased cholesterol accumulation at the cell surface during metaphase (11). By contrast,
77 Misselwitz and colleagues proposed that physical obstacles and forces that occur during the
78 process of NSS lead to the targeting of topologically prominent sites, such as dividing cells or
79 membrane ruffles (4). Finally, Lorkowski and colleagues have reported that the invasion of *S.*
80 *Typhimurium* at the ruffle site is a highly cooperative effort (12), (6). Indeed, co-infection of
81 WT and non-invasive *S. Typhimurium* mutants resulted in the entry of both strains inside the
82 host cells: non-invasive *S. Typhimurium* mutants are trapped at ruffle sites and concomitantly
83 internalized within the host cell, following the active invasion by WT *S. Typhimurium*.
84 However, the cooperative effect between intracellular and entering bacteria remains poorly
85 understood at later stage of the infection.

86

87 An increasing number of studies have highlighted the relevance of intrinsic cellular
88 heterogeneity within eukaryotic monocultures. After seeding, cells display a dynamic range of
89 variability in their morphology depending on their local microenvironment, including the local
90 density, and the peripheral or central positioning within cellular islets (13). This heterogeneity
91 results in differences of transcription (14), (15), lipid composition (15), (13) and sensitivity
92 towards infections (13). Such cell-to-cell variations have been studied during viral infection

93 revealing that simian virus 40 and mouse hepatitis virus present a population-determined
94 pattern of infection associated with differential cell local crowding (13). In the context of
95 bacterial infection, cell targeting has been related to bacterial cooperation at the entry site
96 and evaluated at the whole population level using Colony Forming Unit (CFU) counting or
97 flow cytometry analysis (12), but so far not *in situ* at the single cell level.

98
99 Here we investigated the susceptibility of epithelial host cells within the same cell population
100 to become infected by *S. Typhimurium*. Our analysis revealed that some cells are more likely
101 to be infected by *Salmonella* than others. We termed them “vulnerable cells”. The cell
102 vulnerability was characterized in a quantitative manner by automated high-content imaging
103 through double sequential infections with a delay of 1 to 3 h between the bacterial
104 challenges. The number of intracellular bacteria per cell as well as the corresponding host
105 cell parameters were assessed, such as cell perimeter, local density, and number of infected
106 neighboring cells. Using a mathematical model, we showed that host cell vulnerability can be
107 induced by a first bacterial uptake but also emerged from its intrinsic morphological and
108 micro-environmental characteristics.

109 **RESULTS**

110

111 **Sequential infections allow studies of *Salmonella* cooperation at the single cell level**

112

113 We carried out a microscopy-based double infection assay to explore possible links between
114 host cell vulnerability and successive bacterial infections of epithelial cells (**Fig.1**). HeLa cells
115 grown in 96-well plates were subjected to a first infection with green *S. Typhimurium*
116 expressing the fluorescent protein GFP (SL_{GFP}) for 30 min followed by elimination of the
117 extracellular bacteria via gentamicin treatment and washing. The cells were then incubated
118 for 1, 2 or 3 h before being subjected to a second wave of infection with red *S. Typhimurium*
119 expressing the fluorescent protein dsRed (SL_{dsRed}). Extracellular bacteria were again
120 eliminated in the same way, and the host cells were stained with CellMask and DAPI before
121 automated image acquisition of the entire culture wells (**Fig.1A**). The obtained images were
122 analyzed with CellProfiler, a widely used image analysis software (16), (17) (**Fig.1B**). The
123 differently labeled bacteria and the stained host cells enabled us to distinguish and quantify
124 distinct cellular populations: those cells infected during the 1st infection (I₁) or not (noI₁), those
125 infected during the 2nd infection (I₂) or not (noI₂), as well as the associated subpopulations
126 (I₁&I₂, noI₁&noI₂, I₁&noI₂ and noI₁&I₂) (**Fig.1C**). We based our analysis on comparing the
127 probabilities of infection in these subpopulations.

128

129 ***Salmonella* cooperates for entry at ruffles**

130

131 In order to test the reliability of our method, we analyzed first if we could detect the ruffle-
132 dependent cooperation between individual salmonellae during host cell entry, previously
133 observed in infected HeLa and MDCK cells (4), (12). To do this we determined first the time
134 window during which ruffle-associated cooperation could potentially occur by performing
135 time-lapse microscopy of *Salmonella* infection of HeLa cells transiently expressing GFP-
136 tagged actin (**Fig. 1D**). Time series of 90 min at 3 min intervals provided image sequences
137 with forming and disappearing ruffles. In most of the cases, we observed the uptake of one to
138 two bacteria per ruffle, and we saw ruffle disappearance in less than 15 min (**Movie.S1**). We
139 noticed that the more bacteria were engulfed by the ruffles, the longer we could detect the
140 presence of these ruffles. Therefore, newly arriving bacteria prompted additional growth of
141 the ruffles (**Movie.S2**). We quantified the ruffle lifetime by measuring the delay of their
142 disappearance after the entry of the last bacterium. The few cases of very high infection (>5
143 bacteria/ruffle) that could not be properly analyzed were excluded. Quantification revealed an
144 average ruffle lifetime of 13 min and that 90% of the ruffles completely disappeared after 24
145 min (**Fig.1D**). Labeling Caco-2 cells with the membrane dye FM 4-64, we observed that the
146 ruffle lifetime for infected Caco-2 cells were similar to infected HeLa cells.

147

148 We then challenged HeLa and Caco-2 cells with SL_{GFP} and SL_{dsRed} at the same time and
149 compared the probability for SL_{dsRed} to infect the same cell containing simultaneously SL_{GFP}
150 with those that did not contain SL_{GFP} (**Fig.1E;F;G**); see *Materials and Methods* for details.
151 The probability of SL_{dsRed} infection was significantly higher in a cell infected by SL_{GFP} than in
152 a cell not infected by SL_{GFP} , both for HeLa (**Fig.1E**) and Caco-2 (**Fig.1F**) cells. The repartition
153 of the different populations of infected cells shows a much larger overlap between the cells
154 co-infected with SL_{GFP} and SL_{dsRed} than one would anticipate theoretically for two
155 independent infections (**Fig.1G**). Thus, the efficiency of *Salmonella* invasion of an individual
156 epithelial cell depends on the concomitant invasion of the same cell by other salmonellae.
157 Interestingly, increasing the multiplicity of infection (MOI) in HeLa cells (**Fig.1E**) resulted in a
158 significant increase of the SL_{dsRed} infection in cells infected by SL_{GFP} , but not in cells not
159 infected by SL_{GFP} . This result confirmed that the direct effect of an MOI increase is a higher
160 number of bacteria that infect certain cells rather than an increase in the overall number of
161 cells that become infected. In addition to the previously reported *Salmonella* cooperative
162 entry in HeLa and MDCK cells (4), (12), we showed here that this cooperation also takes
163 place in Caco-2 cells, suggesting that this phenomenon is universal during *Salmonella* entry
164 in epithelial cells. Taken together, these results validated that our system was operational.

165
166
167
168

The probability of being re-infected by *Salmonella* is higher for already-infected cells, even after the disappearance of the entry ruffles

169 To study long-term and ruffle-unrelated cooperative events of *Salmonella* co-infections, we
170 set up the sequential infections with a delay of 1 h between the two infection waves, killing
171 extracellular bacteria in between through gentamicin treatment. Scanning our time-lapse
172 movies, we were ensured that this time lag led to the complete disappearance of any
173 remaining entry ruffles from the first infection. In addition, we extended the delay between the
174 two sequential infections to 2 h and 3 h (see **Fig.1A**). We compared the different populations
175 of cells infected during the 2nd infection (population I_2), depending on whether they were
176 already infected during the first wave of infection (population $I_2 | I_1$) or not (population $I_2 | \text{not } I_1$)
177 for HeLa (**Fig.2A**) and Caco-2 (**Fig.2B**) cells. For both tested cell types, it was significantly
178 more probable for a cell infected the 1st time to be re-infected the 2nd time compared to a cell
179 not previously infected. We propose that such cells are somehow more vulnerable for future
180 infection.

181

182 During all sequential infection experiments we also controlled the overall infection efficiencies
183 of SL_{GFP} and SL_{dsRed} at all measured time points (1st: SL_{GFP} - 2nd: SL_{dsRed} or in the reverse
184 order) (**Fig.S1**). In all cases, the percentage of cells infected by each fluorescent *Salmonella*
185 was similar to cells subjected to single (control) or sequential infections, underlining that

186 sequential infections did not change the overall infection efficiency for the differently colored
187 salmonellae. Nevertheless, we noticed a decrease in the amount of infected cells between
188 the early infection and later time points. This effect is most likely due to the technically
189 unavoidable gentamicin treatment between infections. Besides, SL_{GFP} showed a higher
190 infectivity than SL_{dsRed} for each condition explained by general deleterious effects of the
191 heterologously overexpressed fluorescent proteins on *Salmonella* infectivity, and by the
192 partial loss of dsRed expression observed by us and others. Taking into account these
193 issues, we took advantage of the observed consistency of the differences of infection
194 efficiency between the initial and the successive infections, and between SL_{GFP} and SL_{dsRed} .
195 This consistency allows comparative analyses of the ratio of the different infection
196 probabilities, and it provided us with an analytical tool for precise quantification independently
197 of the variances of the differently colored bacteria and technical hurdles of sequential
198 infection.

199

200 We defined a “vulnerability score” as the conditional probability for a cell to be infected during
201 the 2nd infection after it had already been infected during the 1st one ($I_2 | I_1$), divided by the
202 conditional probability for a cell to be infected during the 2nd infection when it had not been
203 previously infected ($I_2 | \text{no}I_1$) (described in details in *Materials and Methods*). We also
204 analyzed the changes of the vulnerability score in time comparing cells subjected to
205 sequential infections with 1, 2 and 3 h delays (**Fig.2B** and **Fig.S2** for detailed representation
206 of the conditional probability for each replicate). Surprisingly, the vulnerability score appeared
207 un-altered. We obtained similar results when reversing the order of the tested pathogens,
208 infecting first with SL_{dsRed} and then with SL_{GFP} (**Fig.S3**). It was not possible to shorten the
209 delay between infections to less than 1 h due to the ruffle influence, and we could not extend
210 it beyond 3 h due to potential release of hyper-replicative (HR) bacteria from the first infection
211 into the extracellular medium that could then re-infect new cells during the 2nd wave of
212 infection. Altogether, these results showed that, after ruffle disappearance, the infected cells
213 remain more vulnerable to a new infection than the non-infected ones, and this vulnerability
214 is stable in time.

215

216

217 **Cell vulnerability to secondary infection can be predicted from the number of** 218 **intracellular bacteria**

219

220 So far, we only considered the character “infected” or “non-infected” for each cell after SL_{GFP}
221 and SL_{dsRed} infections that provides global trends on their interaction. To further exploit our
222 data we quantified the number of bacteria per host cell and related the obtained numbers
223 with the previously extracted vulnerability scores. The distribution of intracellular bacteria

224 inside infected cells at 2.5 h post-infection (p_i) showed that most of the cells contained a few
225 bacteria, and the proportion of cells decreased drastically when the number of intracellular
226 bacteria increases. Overall, we were able to distinguish three groups of infected cells: the
227 ones containing one to two intracellular bacteria (35% of the global population), the ones
228 containing three to eight intracellular bacteria (39% of the global population) and the ones
229 containing more than nine intracellular bacteria (26% of the global population), corresponding
230 respectively to low, medium and high infections (**Fig.3A**).

231

232 We compared the vulnerability score of these three infection groups during sequential double
233 infections (**Fig.3B**). This analysis revealed that the more bacteria had entered in a given host
234 cell during the first infection, the more it was likely that this cell became re-infected. Such
235 tendencies still emerged when the bacteria were not grouped, but analyzed individually,
236 underlining the robustness of this result (**Fig.S4**).

237

238 Then, we investigated how the level of bacterial uptake during the second infection depends
239 on the number of intracellular bacteria of the first infection. For this we quantified the
240 probability for a cell to be highly infected during the second infection as a function of the
241 efficiency of the first uptake (**Fig.3C**). We found that the more intracellular bacteria had been
242 internalized during the first infection, the more likely the host cells were to engulf a high
243 amount of new bacteria during the second infection. Therefore, we propose that cell
244 vulnerability is maintained from the first to the second infection.

245

246 **Cell vulnerability as intrinsic or induced property**

247

248 The results from the sequential infections (**Fig.2** and **Fig.3**) provided quantitative scores of
249 cell vulnerability towards *Salmonella* infection. We secondly investigated the origin of the
250 observed cell vulnerability. Two possibilities can be anticipated: (i) the cellular vulnerability
251 would be an intrinsic host cell attribute (hypothesis 1: "intrinsic vulnerability") or (ii) it would
252 be induced by bacterial uptake (hypothesis 2: "induced vulnerability") (**Fig.4A**). In theory,
253 these hypotheses can be distinguished by the observable difference in the probability of the
254 2nd wave of infection occurring in previously non-infected cells $P(I_2 | noI_1)$ as depicted in the
255 two schemes of **Fig.4B** and described as follows: In the case of vulnerability as intrinsic
256 attribute, the probability of infection $P(I_2 | noI_1)$ would be lower than $P(I_{2Ctr})$ as the pool of
257 vulnerable cells would have already been partially consumed during the 1st sequential
258 infection, whereas it would remain conserved in the control (**Fig.4B-left**). In the case of
259 induced vulnerability, the probability of infection $P(I_2 | noI_1)$ would be similar to $P(I_{2Ctr})$, as the
260 cells would be considered with equivalent vulnerabilities before their first infection (**Fig.4B-**
261 **right**). The experimental data obtained did not show a significant difference between $P(I_2 |$

262 n_{I_1}) and $P(I_{2Ctr})$ (t-test p-value >0,05) (**Fig.4C**), suggesting that vulnerability may be induced
263 by bacterial uptake (**Fig.4B**, *hypothesis 2*). Taking into account the small percentage of cells
264 belonging to the studied subpopulations we caution that the absence of a statistically
265 significant difference between these populations did not allow to exclude the first hypothesis
266 of host cell inherent vulnerability.

267

268 **Single cell vulnerability to *Salmonella* infection is a combination of intrinsic and** 269 **induced vulnerability**

270 Considering that the subpopulation comparison could not exclude an involvement of inherent
271 vulnerability, we developed a mathematical model to evaluate the relative contribution of
272 induced and inherent vulnerability to the overall cell vulnerability towards *Salmonella*
273 infection. To investigate the contribution of cell parameters at a single-cell level, we
274 measured different intrinsic variables that could influence the cellular vulnerability, namely
275 the cell morphology (cell perimeters, cell circularity), the local environment (local cell density,
276 number of infected and non-infected neighboring cells), and the above-analyzed features of
277 the *Salmonella* infection (delay between infections, load of intracellular bacteria per cell from
278 I_1) (**Fig.5A**). We extracted all these elements using Icy, an image analysis software (18)
279 being recently used for *Salmonella* infection studies *in situ* (19) (see **Fig.S5A** for illustration
280 of Icy cell segmentation).

281

282 First, we analyzed the distribution of distinct cellular parameters in either infected or in non-
283 infected HeLa (upper panels) and Caco-2 (lower panels) cell populations (**Fig.5A**). Caco-2
284 cells were cultured at high confluence so that the cells formed a continuous polarized
285 monolayer (see *Materials and Methods*). For both cell types, the infected cells displayed
286 distinct cellular features in comparison to the non-infected cells, such as a higher local
287 crowding reflected by a higher number of neighboring cells in direct contact. Comparing the
288 relative correlations of the cellular parameters, we highlight the presence of strong links
289 between many of them (**Fig.S5B-C, S6 and S7**). In particular cell morphology is highly
290 dependent on the local micro-environment, such as the local cell density that negatively
291 correlates with the cell perimeter in HeLa and Caco-2 cells. Interestingly, cells that were
292 infected during the second bacterial challenge are more likely to be nearby cells that were
293 infected during the first bacterial challenge (“infected neighbor cells”) than by non-infected
294 neighbor cells. Thus *Salmonella* infection of one cell increases the probability of its
295 neighboring cells to be subsequently infected.

296

297 To quantify the direct involvement of each studied parameter on the overall cell vulnerability
298 we developed a statistic modeling approach adapted to our high-throughput microscopy
299 dataset on sequential *Salmonella* infection. This model is based on a logistic regression that
300 is able to predict the infection efficiency at a single cell level from cellular parameters. We
301 measured the contribution of each parameter to the prediction by estimating how well the
302 model predicts compared to a model that would ignore one parameter; as described in
303 *Materials and Methods (Fig.5B)*. Taken separately, the load of intracellular bacteria resulting
304 from I_1 directly improved the prediction of cell vulnerability towards subsequent infection
305 (**Fig.5B**). Thus, host cell vulnerability is induced by bacterial uptake, which is in line with our
306 experimental data. In addition, the host cell parameters linked to cell morphology and local
307 environment also significantly improved the model prediction of infection for HeLa and for
308 Caco-2 cells (see **Table.S1** and **Table.S2** for model details and the value of the coefficients).
309 Together, our modeling approach revealed that single host cell vulnerability to *Salmonella*
310 infection is a combination of intrinsic and bacterial-induced vulnerability.

311 We quantified their relative involvement by calculating the model-based fold change in the
312 probability of infection of a cell not infected and having a low score of inherent vulnerability
313 with a cell infected and/or having a high score of inherent vulnerability (**Fig.5C**). This showed
314 that induced and intrinsic vulnerability have both a strong impact on the overall cell
315 vulnerability. Interestingly, the induced vulnerability is more prevalent for *Salmonella* infection
316 of HeLa cells (2.2 fold-increase) than infection of Caco-2 cells (1.3 fold-increase), whereas
317 the inherent vulnerability plays a more prominent role for Caco-2 cell infections (2,6 fold-
318 increase) than for HeLa cells (1.6 fold-increase). From these findings we conclude that the
319 analyzed host cell parameters are differentially involved in relation to cell vulnerability
320 towards *Salmonella* infection depending on the cell type. In particular, the local cell density
321 increases the cell vulnerability for HeLa cells but reduces it for Caco-2 cells (**Fig.5D**). This
322 could be explained by the polarization of the Caco-2 at high confluence and highlights the
323 specificity of each predicted model for a given cell-type.

324 We also investigated whether the first infection affects the inherent host cell parameters, we
325 compared the correlation between parameters that were identified as being either involved or
326 not involved in the inherent vulnerability of the cell (**Fig.S8**). As their correlations were similar
327 in infected and non-infected cells we concluded that *Salmonella* infection did not impact the
328 implication of the studied inherent cell parameters.

329

330 **Reliability of the model-based prediction of infection**

331 To investigate the spatial distribution of the cell vulnerability among the cell population, we
332 generated “vulnerability maps” from the original images of the cell population after labeling

333 each cell nucleus with a color corresponding to its probability of infection (**Fig.6A**). Notably,
334 we could confirm that on average the infected cells were properly assigned with a higher
335 prediction score to be infected than the non-infected ones (see **Fig.S9** for *quantification*).
336 Based on our vulnerability maps, the predicted infected cells showed a very good overlap or
337 were in close vicinity with the experimentally infected cells (**Fig.6A**). This illustrates the
338 reliability of our approach in a qualitative way, and it also underlines the impact of local
339 micro-environment on cell vulnerability. We went on to quantify the veracity of the HeLa and
340 Caco-2 adapted models when confronted with 100 experimentally measured infected and
341 100 experimentally measured non-infected cells. For both cell-types, models allowed a good
342 prediction in the majority of the cases, 62% for HeLa and 66% for Caco-2, respectively
343 (**Fig.6B**). Taken together, these results attest that the probability of *Salmonella* infection
344 success can be forecast at the near single-cell level based on host cell parameters.

345

346 **Involvement of cellular cholesterol level as an inherent vulnerability factor**

347 To investigate the molecular players that are linked to the inherent cell vulnerability towards
348 *Salmonella* infection, we analyzed the plasma membrane composition as a main feature
349 known to be relevant to *Salmonella* infection. We focused on cholesterol as the cells at low
350 crowding present a higher amount of free cholesterol than the cells at high crowding (15). We
351 monitored the relationship between global cellular cholesterol levels and host cell targeting
352 performing *Salmonella* infection of HeLa cells for 30 min, followed by cholesterol labeling via
353 filipin staining. Although filipin is the most commonly used tool to assess cholesterol content,
354 it also displays very fast photobleaching properties (20). Thus, the automatic acquisition of
355 an entire 96-wells plate would introduce a strong bias due to the loss of filipin signal during
356 the acquisition. To circumvent this technical issue, we carried out flow cytometry acquisition
357 and analysis (**Fig.7**). For each experiment, we binned the total cell population into five
358 subpopulations corresponding to the increasing cellular levels of cholesterol that we
359 classified as 1 to 5, with each subpopulation containing 20% of the total cells (see **Fig.S10**
360 for *FACS gating details*). Comparing the number of infected cells in these different
361 subpopulations with different amounts of cholesterol in HeLa (**Fig.7A**) and Caco-2 (**Fig.7B**)
362 cells, we revealed that the probability of infection correlates in both cases with the cholesterol
363 levels. Increasing the cholesterol level corresponds to a decrease of the probability of
364 *Salmonella* infection in HeLa cells (**Fig.7A**), however it also corresponds to an increase of
365 the infection in Caco-2 cells (**Fig.7B**). Thus, similarly to the cell density, the cholesterol level
366 is a host cell parameter allowing to estimate the cell vulnerability towards *Salmonella*
367 infection in a cell-type dependent manner.

368 **DISCUSSION**

369
370 Cellular heterogeneity describes cases in which genetically identical cells present different
371 behaviors and morphologies. This biological phenomenon is commonly present in an
372 epithelial layer of an individual as well as within a monolayer of cultured cells. Despite the
373 realization of the importance of cellular heterogeneity, its study has only become feasible
374 during recent years, mainly thanks to the implementation of novel technologies such as
375 imaging and computer-assisted analyses. In the context of pathogen infection, this
376 heterogeneity produces cells unequally vulnerable or resistant, which impacts on the overall
377 infection.

378

379 We investigated the cell vulnerability of epithelial cells for *S. Typhimurium* infection.
380 According to our results, infected cells display a strikingly higher probability of being re-
381 infected with *Salmonella*, even after the disappearance of membrane ruffles. We obtained
382 similar results in two relevant epithelial cell lines, HeLa and Caco-2, suggesting that this
383 represents a conserved propensity towards *Salmonella* infection. The measured cellular
384 vulnerability remained unaltered for all measured time-points ranging from a delay of 1 h to 3
385 h between the infections. Attributing a “vulnerability score” to the challenged cells, we
386 showed a higher vulnerability score in cells that had been previously infected, and we found
387 that this score increased with the amount of intracellular bacteria contained by a given cell.
388 This result raises the issue of the bacterial impact on the cell vulnerability. Therefore, we
389 aimed at distinguishing inherent cell vulnerability from the one induced by bacterial uptake
390 (**Fig.4A**, *hypothesis 1 and 2 respectively*) exploiting the imaging data obtained via a high-
391 content analytical pipeline. This allowed visualization of the infection *in situ* and provided a
392 large number of associated cellular parameters. We quantified the implication of specific
393 parameters associated with individual cells on the cell vulnerability towards *Salmonella*
394 infection. It appeared clearly that the efficiency of early bacterial uptake during the first
395 infection directly determines cell vulnerability. Thus *Salmonella* induces an increase in the
396 cell vulnerability towards subsequent infections.

397 While long-term cooperation among bacteria has been extensively studied for the
398 communities of bacteria living in a common extracellular environment (21), little is known
399 about the cooperation between intracellular and extracellular bacteria leading to increased
400 bacterial uptake. Nevertheless, this phenomenon has been investigated more extensively for
401 many viruses, including bacteriophages (22), influenza virus (23), poxviruses (24, 25),
402 flaviviruses (26, 27) alphaviruses (28), and alphaherpesviruses (29). Generally, those works
403 have demonstrated that the first virus to infect a cell has the capacity to prevent co-infection
404 of other viruses belonging either to the same strain, or to more distantly related or unrelated

405 strains. It is termed “superinfection exclusion” and may protect limited cellular resources and
406 promote the replication and dissemination of the originally infecting virus. By analogy, the
407 increased probability of cellular re-infection by *Salmonella* can be phrased as a
408 “superinfection promotion”. It remains to be clarified if such process is relevant for all
409 intracellular bacteria. For instance and in contrast to *Salmonella* infection, Jorgensen *et al*
410 reported that the *Chlamydia* effector protein CPAF secreted from bacteria within mature
411 inclusions prevents those that are still extracellular to invade (30). Thus, CPAF could be a
412 factor mediating *Chlamydia* resistance towards superinfection.

413

414 Our approach also allowed the relative quantification of the impact of different host cell
415 parameters on the inherent vulnerability of host cell to *Salmonella* infection. In particular,
416 morphological attributes and local cell crowding are highly linked with this vulnerability. Cell
417 crowding as a major determinant for the probability to become infected has been proposed
418 by Snijder and colleagues in the context of viral infection. They showed that during infections
419 by the simian virus SV40 or the mouse hepatitis virus (MHV), the targeted cells have different
420 localization within cell islets (13). SV40 and MHV infect preferentially either peripheral or
421 central cells, a phenomenon that is linked to the differential expression levels of focal
422 adhesion kinase and the presence of sphingolipid GM1 at the plasma membrane of the
423 challenged host cells. Thus, similarly to several viral infections, the probability of infection of
424 a single cell by *Salmonella* is influenced by its local environment.

425

426 Our analytical tools will be useful for further studies on *Salmonella*, and for other researchers
427 working on different intracellular bacterial pathogens, such as *Chlamydia*, *Listeria* or *Shigella*
428 (see *Materials and Methods*). We revealed that some cells are indeed intrinsically more
429 vulnerable to *Salmonella* and will be targeted by the bacteria first. Most of the tested
430 parameters appeared to be relevant for model-based infection prediction but are differentially
431 involved in the cell vulnerability depending on the cell-type studied. Developing an adapted
432 model based on host cell parameters we could forecast the probability of *Salmonella*
433 infection success at the near single-cell level. Interestingly, the number of infected
434 neighboring cells is highly increased in the population of infected cells. Cases of bacterial
435 uptake impacting on the cells neighboring the infection (called bystander cells) have been
436 previously reported for *Shigella* that induces an IL-8 immune response after NF κ B activation
437 detectable from 2 h pi in 70% of the bystander cells (31). However, it is not known whether
438 the neighboring cells are also more susceptible to *Shigella* entry.

439

440 Because of our lack of knowledge of host factors that are involved in the early attachment,
441 such as potential entry receptors, it remains difficult to identify the molecular mechanisms

442 that establish the differential vulnerability during *Salmonella* infection. Although receptors for
443 direct recognition of *Salmonella* have been proposed, such as the cystic fibrosis
444 transmembrane conductance regulator (CFTR) (32) and the epithelium growth factor
445 receptor (EGFR) (33), many cell types infected by *Salmonella* do not express them (34).
446 Therefore, it has been proposed that recognition mechanisms likely involve more ubiquitous
447 factors (35). To explore the molecular cues involved in the inherent heterogeneity of host cell
448 vulnerability, we decided to investigate the membrane lipid composition, in particular cellular
449 cholesterol. We found that the cholesterol amount at single cell level in HeLa and Caco-2
450 cells correlates with the vulnerability of these cells to *Salmonella* infection. In HeLa cells
451 *Salmonella* preferentially targets cells with low amounts of cholesterol. However, in Caco-2
452 cells, *Salmonella* preferentially targets cells with high amounts of cholesterol. Interestingly,
453 these results on an implicated host molecule are in agreement with the morphological feature
454 of local density. Frechin and colleagues reported that cells at high density contain lower
455 amounts of cholesterol (15). Besides, at high density HeLa and Caco-2 cells display an
456 increase or a decrease in inherent cell vulnerability, respectively. This is in line with the
457 correlation that we reported between the cholesterol level and host cell vulnerability. The
458 molecular role of cholesterol during *Salmonella* infection is still under debate. Several studies
459 have demonstrated that the *Salmonella* SipB effector and translocon component requires
460 cholesterol for proper functioning (35, 36). In this context, it should be noted that the
461 translocons operate in small cholesterol-rich microdomains at the plasma membrane and
462 cannot be linked readily to the overall cholesterol levels. Furthermore, those studies were
463 based on sterol sequestering agents and biosynthesis inhibitors. Contrastingly, Gilk and
464 colleagues have shown that cholesterol is not essential for *Salmonella* invasion and
465 intracellular replication inside host cells using an original mouse model (37). In our study we
466 highlighted that non-treated HeLa cells with a low amount of global cellular cholesterol are
467 preferentially targeted by *Salmonella*, which does not exclude a potential involvement of
468 cholesterol at the subcellular level. Santos and colleagues have also reported that the
469 preferential invasion of hTERT-RPE1 and HeLa mitotic cells by *Salmonella* was SipB and
470 cholesterol dependent (11). However, the low amount of mitotic cells in the whole population
471 (< 4%) may have a limited impact on the overall inherent vulnerability of the host cell
472 population. Thus our observation that the most vulnerable HeLa cells display a low
473 cholesterol level is not in contradiction with previous publication on cholesterol involvement
474 during *Salmonella* infection process.

475

476 In conclusion, our study represents a first step in understanding *Salmonella* cell targeting and
477 provides a path for the identification of cellular and bacterial factors involved in host cell
478 vulnerability. Such factors could be targeted to render a cell more resistant to pathogen

479 infections, allowing potential new therapeutic strategies. Together, our study delineates in a
480 quantitative manner the importance of vulnerable cell recognition and bacterial cooperation
481 for cell targeting by *S. Typhimurium*.

482 **MATERIALS AND METHODS**

483

484 **Bacterial Strains**

485 The following *S. Typhimurium* were used: SL1344 (wild type), SL1344 pM965 (*Salmonella*-
486 GFP) described by Stecher *et al* (38), and SL1344 pGG2 (*Salmonella*-dsRed) obtained after
487 transformation of SL1344 with the pGG2 plasmid described by Lelouard *et al* (39). Bacteria
488 were grown in Lysogeny Broth (LB) medium supplemented with 0.3 M NaCl and ampicillin at
489 50 µg/ml at 37°C in an orbital shaker.

490

491 **Cell Culture**

492 All cell culture reagents were purchased from Invitrogen unless otherwise stated. Human
493 epithelial HeLa cells (clone CCL-2 from ATCC) were cultured in Dulbecco's Modified Eagle's
494 Medium (DMEM) supplemented with 10% (v/v) fetal bovine serum (FBS), at 37 °C, 5% CO₂.
495 HeLa cells were plated at a concentration of 1.5x10⁴ cells/well in glass-bottom 96-wells
496 plates 24 h before infection, so that they displayed about 80% of confluence on the infection
497 day. Intestinal epithelial Caco-2 TC7 cells (kindly provided by P. Sansonetti) were grown in
498 DMEM supplemented with 10% FBS at 37°C, 10% CO₂. Caco-2 cells were plated at a
499 concentration of 3.5x10⁴ cells/well in glass-bottom 96-wells plates 48 h before infection, so
500 that they displayed a polarized (but not differentiated) continuous monolayer on the infection
501 day. All infection assays were performed in EM buffer (120 mM NaCl, 7 mM KCl, 1.8 mM
502 CaCl₂, 0.8 mM MgCl₂, 5 mM glucose, 25 mM HEPES, pH 7.4). HeLa cells were transfected
503 with pEGFP-actin plasmid DNA (40) from a maxiprep, using the X-tremeGENE 9 DNA
504 transfection reagent (Roche) for 48 h.

505

506 **Double Infection Assays**

507 For invasion experiments, overnight bacterial cultures were sub-cultured 1/20 and grown until
508 late exponential/early stationary phase. Before infection, bacteria were gently washed and
509 resuspended in EM buffer. Bacteria were added to the cells at an MOI of 30 corresponding to
510 CFU, and incubated for 30 min at 37 °C, 5% or 10% CO₂ for HeLa or Caco-2 cells,
511 respectively. Non-internalized bacteria were eliminated by washing 3 times with warm EM
512 buffer and incubated for 1, 2 or 3 h at 37 °C, 5% or 10% CO₂ for HeLa or Caco-2 cells,
513 respectively. Adding EM buffer containing 100 µg/ml gentamicin for 1 h killed extracellular
514 bacteria. The concentration of gentamicin was then decreased to 10 µg/ml and 10% FBS
515 was added to the medium. At the desired time points, the cells were washed again in EM
516 buffer to eliminate the remaining gentamicin and re-infected with a fresh batch of sub-
517 cultured bacteria following the same protocol. After killing the extracellular bacteria again by

518 a 1 h of incubation with EM buffer containing 100 µg/ml gentamicin, the cells were fixed with
519 4% paraformaldehyde at room temperature for immunofluorescence analysis.

520

521 **Microscopy**

522 All image acquisitions were performed on a Nikon inverted widefield microscope using a
523 20x/0.5NA air objective, an automatic programmable XY-stage and the Nikon perfect focus
524 system. For sequential infections of HeLa and Caco-2 cells, 161 fields were imaged per well
525 and four channels per field were captured using a CoolSnap2 camera (Roper Scientific).
526 Nuclei and cells were stained using DAPI (excitation/emission wavelengths: 350/470 nm)
527 and the cell bodies with CellMask DeepRed Plasma Membrane Stain
528 (ThermoFisherScientific, excitation/emission wavelengths: 640/670 nm) respectively. Caco-2
529 cells were stained with the FM® 4-64 membrane dye (Invitrogen) before time lapse imaging
530 (excitation/emission wavelengths: 558/734 nm). Quantification of the ruffle timing was
531 performed on the same microscope, using a 20x/0.5NA air objective and time intervals of 3
532 min for 90 min. Time lapse imaging of ruffles was performed on a DeltaVision widefield
533 microscope using a 60x/1.42 NA oil objective and z-stacks with a spacing of 500 nm. The
534 images were subsequently de-convolved using DeltaVision Elite integrated software.

535

536 **Cholesterol measurements**

537 HeLa and Caco-2 cells were challenged with SL_{GFP} for 30 min before trypsinization, fixation
538 with 4% paraformaldehyde at room temperature and incubation with 16ug/mL filipin complex
539 from *Streptomyces filipinensis* (Sigma-Aldrich). This treatment was directly followed by FACS
540 measurement on *BD FACS CANTO* cytometer using the excitation/emission wavelengths of
541 405/450 nm and 488/530 nm for filipin and GFP fluorescence detection respectively. Infected
542 and non-infected cells were distinguished using the green fluorescence emitted by SL_{GFP}
543 (see **Fig.S10** for gating details). Data were processed using FlowJo software.

544

545 **Image Analysis**

546 All images were analyzed with two open source software: CellProfiler (<http://cellprofiler.org/>)
547 and Icy (<http://icy.bioimageanalysis.org/>). CellProfiler was used to detect each single cell
548 and the number of its intracellular salmonellae expressing either GFP or dsRed. The
549 following modules were used during the analysis: *IdentifyPrimaryObjects* recognized nuclei
550 and bacteria; *IdentifySecondaryObjects* identified cells (here the secondary objects) by
551 extending the nuclear area previously recognized; *RelateObjects* assigned bacteria within
552 individual cells. Icy was used for accurate detection of cell borders and the cellular
553 microenvironment analysis. We used a graphical environment called *Protocols* for the
554 development of an analytical pipeline including the following plugins: *HK-Means* that identify

555 nuclei by pre-filtering the signal to identify objects within a size range; *Spot Detector* that
 556 identify bacteria; *Active Contours* that identify the edges of the plasma membrane by
 557 propagating the Region of Interest (ROI) detected for the nuclei; and *Javascript* that parent
 558 the ROI of cells with bacteria, to measure local cell density and to distinguish which
 559 neighboring cells are infected by which bacteria.

560

561

562 **Probability**

563 $P(I_2|I_1)$ means “Probability of the 2nd sequential infection, knowing that the cell has been
 564 infected by the 1st one” and is calculated as follows:

$$565 \quad P(I_2|I_1) = P(I_1 \& I_2) / P(I_1)$$

566 Where $P(I_1) = [\text{Number of cells in } I_1 / \text{Total number of cells}]$, and $P(I_1 \& I_2) = [\text{Number of cells in } I_1 \& I_2 / \text{Total number of cells}]$.

567

569 $P(I_2|noI_1)$ means “Probability of the 2nd sequential infection, knowing that the cell has not
 570 been infected by the 1st one” and is calculated as follows:

$$571 \quad P(I_2|noI_1) = P(I_2 \& noI_1) / P(noI_1)$$

572 Where $P(noI_1) = [\text{Number of cells in } noI_1 / \text{Total number of cells}]$, and $P(I_2 \& noI_1) = [\text{Number of cells in } noI_1 \& I_2 / \text{Total number of cells}]$.

573

574 **Model**

575 We modeled the influence of multiple parameters on the probability of a second infection. A
 576 Boolean variable Y represents the second infection: It is equal to 1 for infected cells and 0
 577 otherwise. Its probability is predicted by the following seven parameters: *Load of infection*
 578 (LOI) represents the number of infecting bacterium during the first infection, separated in 4
 579 groups corresponding to no (0 bacteria), low (1 or 2), medium (3 to 8) or high (9+)
 580 infection. *Delay* is a categorical variable corresponding to the delay between the 1st and the
 581 2nd infections (1, 2 or 3 h). *Infected neighbor cells* (X_1) refers to the number of cells in
 582 contact that had been infected during the first infection. *Non-Infected neighbor cells*
 583 (X_2) refers to the number of cells in contact which had not been infected during the first
 584 infection. *Local Cell Density* (X_3) is the number of cells present in a vicinity of 100 μm . The
 585 distance is calculated between the center of the nuclei. *Cell perimeter* (X_4) is the length of
 586 the perimeter of the cell (in μm) obtained after segmentation. *Circularity* (X_5) refers to the cell
 587 circularity defined as: “ $4\pi \cdot \text{area} / \text{perimeter}^2$ ”. This parameter is higher for circular cells, and
 588 lower for cells that are elongated or have complex shape, but does not depend *a priori* on the
 589 cell size. In practice we used to its square root. The probability of Y during the second
 590 infection is modeled as:

$$592 \quad P(Y = 1 | X_1, \dots, X_n) = 1 / [1 + \exp(-(\mathbf{a}LOI + \mathbf{a}Delay + \mathbf{a}_1 X_1 + \dots + \mathbf{a}_5 X_5))]$$

593 where a_{LOI} (resp. a_{Delay}) has a different value for each of the LOI categories (resp. Delay
594 categories), and a_1, \dots, a_5 are constants. All parameters were learned by maximizing the
595 likelihood of the model, e.g. the probability of the observed data as measured by the
596 model. We used 115 000 and 327 000 cells to train and test the model for HeLa and Caco-2
597 cells respectively. We divided the cell population into two random sets; the training set
598 (9/10th of the cells per replicate) and testing set (1/10th of the cells) and computed the
599 likelihood of infection observed in the testing set. The higher the likelihood, the better the
600 parameters of the model predicted infection. We repeated this procedure 100 times. To
601 measure the improvement of infection prediction by taking into account each parameter, the
602 likelihood of the complete model was compared (on a log scale) with the likelihood of seven
603 models ignoring each time one parameter. This difference of log-likelihood is reported
604 in **Fig.5B**.

605 Quantification of the impact of a parameter towards cell vulnerability was obtained by
606 applying our statistical model to the 1st and the 3rd quantile values of a given parameter, while
607 other parameters were kept equal at their median values. We obtained the probabilities of
608 the second infection for these two sets and reported their ratio. In **Fig.5D**, the arrows “↗” and
609 “↘” correspond to a ratio above and under 1 respectively. The parameters-values
610 corresponding to a low inherent vulnerability of HeLa and Caco-2 cells were the following:
611 local cell density (1st quantile and 3rd quantile respectively), cell perimeter (1st quantile),
612 infected neighboring cells (median), non-infected neighboring cells (median), circularity
613 (median and 3rd quantile respectively). The parameters-values corresponding to a high
614 inherent vulnerability of HeLa and Caco-2 cells were the following: local cell density (3rd
615 quantile and 1st quantile respectively), cell perimeter (3rd quantile), infected neighboring cells
616 (median), non-infected neighboring cells (median), circularity (median and 1st quantile
617 respectively).

618 Models reliability was evaluated using 100 infected and 100 non-infected cells and
619 quantifying the amount of “good predictions” among those cells. We repeated this procedure
620 100 times and showed the average. As a comparison, a random model would provide
621 approximately 50% of “good predictions”.

622

623 **Statistical analysis**

624 The statistical analysis was performed using R and GraphPad Prism. T-tests were used to
625 evaluate the significance of the results, referred like *, **, *** for p-values <0.05, <0.01, and
626 <0.001, respectively.

627

628 **Supplemental information**

629 The pipeline used on CellProfiler and on ICY, as well as the R code used to generate the
630 model can be provided by the authors.

631 **ACKNOWLEDGMENTS**

632

633 We thank Jennifer Fredlund and Andrew Rutenberg for their help during the initial phase of
634 the project, Adrien Sauvaget, Claude Loverdo, Kristine Schauer and Uriel Hazan for
635 productive discussions, Mariana Ferrari for her help with the FACS experiments and all the
636 members of the DIHP unit and BioImage Analysis Group for helpful interactions. VS was
637 supported by a Ph.D. fellowship from the University Paris Diderot attributed by the ENS
638 Cachan, Université Paris-Saclay. JE is member of the LabEx consortia IBEID and
639 MilieuInterieur. JE also acknowledges support of from the ANR (grant StopBugEntry and
640 AutoHostPath) and the ERC (CoG EndoSubvert).

641 REFERENCE

642

- 643 1. Majowicz SE, Musto J, Scallan E, Angulo FJ, Kirk M, O'Brien SJ, Jones TF, Fazil A,
644 Hoekstra RM. 2010. The Global Burden of Nontyphoidal Salmonella Gastroenteritis.
645 *Clinical Infectious Diseases* 50:882-889.
- 646 2. Carter PB, Collins FM. 1974. The route of enteric infection in normal mice. *The*
647 *Journal of experimental medicine* 139:1189-203.
- 648 3. Watson KG, Holden DW. 2010. Dynamics of growth and dissemination of Salmonella
649 in vivo. *Cellular Microbiology* 12:1389-1397.
- 650 4. Misselwitz B, Barrett N, Kreibich S, Vonaesch P, Andritschke D, Rout S, Weidner K,
651 Sormaz M, Songhet P, Horvath P, Chabria M, Vogel V, Spori DM, Jenny P, Hardt
652 WD. 2012. Near surface swimming of salmonella Typhimurium explains target-site
653 selection and cooperative invasion. *PLoS Pathogens* 8:9.
- 654 5. Vonaesch P, Cardini S, Sellin ME, Goud B, Hardt WD, Schauer K. 2013. Quantitative
655 insights into actin rearrangements and bacterial target site selection from
656 SalmonellaTyphimurium infection of micropatterned cells. *Cellular Microbiology*
657 15:1851-1865.
- 658 6. Misselwitz B, Kreibich SK, Rout S, Stecher B, Periaswamy B, Hardt WD. 2011.
659 Salmonella enterica serovar typhimurium binds to hela cells via fim-mediated
660 reversible adhesion and irreversible type three secretion system 1-mediated docking.
661 *Infection and Immunity* 79:330-341.
- 662 7. Haraga A, Ohlson MB, Miller SI. 2008. Salmonellae interplay with host cells. *Nature*
663 *Reviews Microbiology* 6:53-66.
- 664 8. LaRock DL, Chaudhary A, Miller SI. 2015. Salmonellae interactions with host
665 processes. *Nature Reviews Microbiology* 13:191-205.
- 666 9. Knodler LA. 2015. Salmonella enterica: Living a double life in epithelial cells. *Current*
667 *Opinion in Microbiology* 23:23-31.
- 668 10. Santos JC, Enninga J. 2016. At the crossroads: Communication of bacteria-
669 containing vacuoles with host organelles. *Cellular Microbiology* 18:330-339.
- 670 11. Santos AJM, Meinecke M, Fessler MB, Holden DW, Boucrot E. 2013. Preferential
671 invasion of mitotic cells by Salmonella reveals that cell surface cholesterol is maximal
672 during metaphase. *Journal of Cell Science* 126:2990-2996.
- 673 12. Lorkowski M, Felipe-López A, Danzer CA, Hansmeier N, Hensel M. 2014. Salmonella
674 enterica invasion of polarized epithelial cells is a highly cooperative effort. *Infection*
675 *and Immunity* 82:2657-2667.

- 676 13. Snijder B, Sacher R, Rämö P, Damm E-M, Liberali P, Pelkmans L. 2009. Population
677 context determines cell-to-cell variability in endocytosis and virus infection. *Nature*
678 461:520-523.
- 679 14. Liberali P, Snijder B, Pelkmans L. 2014. Single-cell and multivariate approaches in
680 genetic perturbation screens. *Nature Reviews Genetics* 16:18-32.
- 681 15. Frechin M, Stoeger T, Daetwyler S, Gehin C, Battich N, Damm E-M, Stergiou L,
682 Riezman H, Pelkmans L. 2015. Cell-intrinsic adaptation of lipid composition to local
683 crowding drives social behaviour. *Nature* 523:88-91.
- 684 16. Carpenter AE, Jones TR, Lamprecht MR, Clarke C, Kang IH, Friman O, Guertin Da,
685 Chang JH, Lindquist Ra, Moffat J, Golland P, Sabatini DM. 2006. CellProfiler: image
686 analysis software for identifying and quantifying cell phenotypes. *Genome biology*
687 7:R100.
- 688 17. Kamensky L, Jones TR, Fraser A, Bray MA, Logan DJ, Madden KL, Ljosa V, Rueden
689 C, Eliceiri KW, Carpenter AE. 2011. Improved structure, function and compatibility for
690 cellprofiler: Modular high-throughput image analysis software. *Bioinformatics*
691 27:1179-1180.
- 692 18. de Chaumont F, Dallongeville S, Chenouard N, Hervé N, Pop S, Provoost T, Meas-
693 Yedid V, Pankajakshan P, Lecomte T, Le Montagner Y, Lagache T, Dufour A, Olivo-
694 Marin J-C. 2012. Icy: an open bioimage informatics platform for extended
695 reproducible research. *Nature Methods* 9:690-696.
- 696 19. McQuate SE, Young AM, Silva-Herzog E, Bunker E, Hernandez M, de Chaumont F,
697 Liu X, Detweiler CS, Palmer AE. 2016. Long-term live-cell imaging reveals new roles
698 for *Salmonella* effector proteins SseG and SteA. *Cellular Microbiology*
699 doi:10.1111/cmi.12641.
- 700 20. Boutte Y, Men S, Grebe M. 2011. Fluorescent in situ visualization of sterols in
701 *Arabidopsis* roots. *Nat Protoc* 6:446-56.
- 702 21. Davey ME, O'toole GA. 2000. Microbial biofilms: from ecology to molecular genetics.
703 *Microbiology and molecular biology reviews* : MMBR 64:847-67.
- 704 22. Cumby N, Davidson AR, Maxwell KL. 2012. The moron comes of age. *Bacteriophage*
705 2:225-228.
- 706 23. Huang IC, Li W, Sui J, Marasco W, Choe H, Farzan M. 2008. Influenza A virus
707 neuraminidase limits viral superinfection. *J Virol* 82:4834-4843.
- 708 24. Doceul V, Hollinshead M, van der Linden L, Smith GL. 2010. Repulsion of
709 superinfecting virions: a mechanism for rapid virus spread. *Science (New York, NY)*
710 327:873-876.

- 711 25. Laliberte JP, Moss B. 2014. A novel mode of poxvirus superinfection exclusion that
712 prevents fusion of the lipid bilayers of viral and cellular membranes. *Journal of*
713 *virology* 88:9751-68.
- 714 26. Zou G, Zhang B, Lim P-Y, Yuan Z, Bernard Ka, Shi P-Y. 2009. Exclusion of West Nile
715 virus superinfection through RNA replication. *Journal of virology* 83:11765-11776.
- 716 27. Schaller T, Appel N, Koutsoudakis G, Kallis S, Lohmann V, Pietschmann T,
717 Bartenschlager R. 2007. Analysis of hepatitis C virus superinfection exclusion by
718 using novel fluorochrome gene-tagged viral genomes. *Journal of virology* 81:4591-
719 603.
- 720 28. Karpf aR, Lenches E, Strauss EG, Strauss JH, Brown DT. 1997. Superinfection
721 exclusion of alphaviruses in three mosquito cell lines persistently infected with
722 Sindbis virus. *Journal of virology* 71:7119-7123.
- 723 29. Criddle A, Thornburg T, Kochetkova I, DePartee M, Taylor MP. 2016. gD-
724 Independent Superinfection Exclusion of Alpha herpesviruses. *Journal of Virology*
725 90:4049-4058.
- 726 30. Jorgensen I, Bednar MM, Amin V, Davis BK, Ting JPY, McCafferty DG, Valdivia RH.
727 2011. The chlamydia protease CPAF regulates host and bacterial proteins to
728 maintain pathogen vacuole integrity and promote virulence. *Cell Host and Microbe*
729 10:21-32.
- 730 31. Kasper CA, Sorg I, Schmutz C, Tschon T, Wischnewski H, Kim ML, Arriemerlou C.
731 2010. Cell-cell propagation of NF- κ B transcription factor and MAP kinase activation
732 amplifies innate immunity against bacterial infection. *Immunity* 33:804-816.
- 733 32. Pier GB, Grout M, Zaidi T, Meluleni G, Mueschenborn SS, Banting G, Ratcliff R,
734 Evans MJ, Colledge WH. 1998. *Salmonella typhi* uses CFTR to enter intestinal
735 epithelial cells. *Nature* 393:79-82.
- 736 33. Pace J, Hayman MJ, Galán JE. 1993. Signal transduction and invasion of epithelial
737 cells by *S. typhimurium*. *Cell* 72:505-514.
- 738 34. Jones BD, Paterson HF, Hall a, Falkow S. 1993. *Salmonella typhimurium* induces
739 membrane ruffling by a growth factor-receptor-independent mechanism. *Proceedings*
740 *of the National Academy of Sciences of the United States of America* 90:10390-
741 10394.
- 742 35. Garner MJ, Hayward RD, Koronakis V. 2002. The *Salmonella* pathogenicity island 1
743 secretion system directs cellular cholesterol redistribution during mammalian cell
744 entry and intracellular trafficking. *Cellular Microbiology* 4:153-165.
- 745 36. Hayward RD, Cain RJ, McGhie EJ, Phillips N, Garner MJ, Koronakis V. 2005.
746 Cholesterol binding by the bacterial type III translocon is essential for virulence
747 effector delivery into mammalian cells. *Molecular Microbiology* 56:590-603.

- 748 37. Gilk SD, Cockrell DC, Luterbach C, Hansen B, Knodler LA, Ibarra JA, Steele-
749 Mortimer O, Heinzen RA. 2013. Bacterial Colonization of Host Cells in the Absence of
750 Cholesterol. *PLoS Pathogens* 9.
- 751 38. Stecher B, Hapfelmeier S, Müller C, Kremer M, Stallmach T, Hardt W-d, Mu C. 2004.
752 Flagella and Chemotaxis Are Required for Efficient Induction of *Salmonella enterica*
753 Serovar Typhimurium Colitis in Streptomycin-Pretreated Mice Flagella and
754 Chemotaxis Are Required for Efficient Induction of *Salmonella enterica* Serovar
755 Typhimurium Colitis. *Infect Immun* 72:4138-4150.
- 756 39. Lelouard H, Henri S, De Bovis Ba, Mugnier Bnd, Chollat-Namy A, Malissen B,
757 M??resse Sp, Gorvel JP. 2010. Pathogenic Bacteria and Dead Cells Are Internalized
758 by a Unique Subset of Peyer's Patch Dendritic Cells That Express Lysozyme.
759 *Gastroenterology* 138:173-184.e3.
- 760 40. Ehsani S, Santos JC, Rodrigues CD, Henriques R, Audry L, Zimmer C, Sansonetti P,
761 Van Nhieu GT, Enninga J. 2012. Hierarchies of host factor dynamics at the entry site
762 of *Shigella flexneri* during host cell invasion. *Infection and Immunity* 80:2548-2557.
763

764 **FIGURE CAPTIONS**

765

766 **Fig.1. Double infections allow studies of *Salmonella* cooperation at the single cell**767 **level. A. B. C.** Overview of the experimental workflow used in this study. **A.** Sequential

768 infection protocol: HeLa cells grown in 96-wells plates since 24 h were subjected for 30 min

769 to a first infection by SL_{GFP}. This was followed by elimination of extracellular bacteria by

770 gentamicin and incubation of the cells for 1, 2 or 3 h. The cells were subsequently challenged

771 by a second infection with SL_{dsRed} for 30 min. After removal of the extracellular bacteria, the

772 samples were fixed. Nuclei were stained with DAPI and cell membranes were stained with

773 CellMask before microscopic acquisition of the entire wells. **B.** Representative image of774 SL_{GFP} and SL_{dsRed} internalized in HeLa cells. Host cell nuclei are visible through DAPI (in775 blue), and cell membranes through CellMask (in grey). Scale bar correspond to 5µm. **C.**

776 Scheme of our statistical analysis of different subpopulations. The following cellular

777 populations can be distinguished: those cells infected during the 1st infection (I₁) or not (noI₁),778 those infected during the 2nd infection (I₂) or not (noI₂), along with the related subpopulations779 (I₁&I₂, noI₁&noI₂). This scheme maps the case of two independent infections. **D.** Time780 distribution of the ruffle disappearance during *Salmonella* infection followed in actin-GFP781 transfected cells by time-lapse microscopy. **E. F.** Comparison of the conditional probability of782 infection for two different populations during synchronous infection of SL_{GFP} and SL_{dsRed}. **E.**783 Results obtained in HeLa cells. **F.** Results obtained in Caco-2 cells. The MOIs were chosen

784 to obtain in average 30% of the cells infected and calculated after CFU counting (n >=3). P-

785 values were obtained after t-test. **G.** Comparison of an independent model (left) with the

786 obtained data (right). The percentages are averaged from 6 independent experiments,

787 represented in **E** with an MOI of 30.

788

789 **Fig.2. The probability of being re-infected by *Salmonella* remains higher for already**790 **infected cells after entry ruffle disappearance. A-B.** Conditional probability of infection for791 two different populations during sequential infection with a delay of 2 h for HeLa cells (**A**) and792 Caco-2 cells (**B**). Results were obtained from 3 independent experiments and P-values were793 obtained after paired t-test. **C.** The vulnerability score was plotted for infection with a 1, 2 or 3794 h delay before the second infection in HeLa cells. The red line corresponds to $P(I_2 | I_1) = P(I_2 |$ 795 $noI_1) = 1$ indicating the independence of the infections I₂ and I₁. Values above the red line796 correspond to $P(I_2 | I_1) > P(I_2 | noI_1)$ indicating a cooperation between infections. Values below797 the red line correspond to $P(I_2 | I_1) < P(I_2 | noI_1)$ indicating a competition between infections.

798 Results were obtained from 3 independent experiments per time-point, and P-values were
799 obtained after unpaired t-test.

800

801 **Fig.3. Cell vulnerability can be predicted from the number of bacteria previously**
802 **internalized. A.** Distribution of the number of intracellular bacteria detected at 1.5 h pi in
803 HeLa cells (average from 3 replicates). The infection efficiencies are clustered in 3 groups:
804 low, medium and high infection, corresponding respectively to 1 to 2; 3 to 8 or more than 9
805 bacteria per cell. **B.** The vulnerability score is represented as a function of the number of
806 intracellular bacteria resulting from the 1st infection in HeLa cells. **C.** Probability of a cell to be
807 highly infected during the 2nd infection ($nI_2 \geq 9$) as a function of the number of intracellular
808 bacteria being internalized during the 1st infection in HeLa cells. **B** and **C** represent the data
809 merged from all the experiments (delay of 1, 2 and 3 h before the second infection). Groups
810 of infection efficiency are identical in **A**, **B** and **C**.

811

812 **Fig.4. Cell vulnerability examined as an intrinsic or an induced property. A.** Schemes of
813 the two hypotheses for the origin of cell vulnerability. In the hypothesis 1, cell vulnerability is
814 inherent: some cells (in orange) are more vulnerable towards infection than other cells (in
815 yellow). In the hypothesis 2, cell vulnerability is induced by bacterial uptake: before infection
816 cells are equal regarding their vulnerability (in yellow), but after infection the infected cells
817 turn progressively more vulnerable (in orange). **B.** Graphic representation of the theoretical
818 distribution of the different populations in the case of hypothesis 1 (left) or hypothesis 2
819 (right). **C.** Probability of infection during sequential infection of HeLa cells with 1, 2 and 3 h
820 delays for control cells (I_{2ctr}) and cells non infected during the 1st infection (noI_1). P-values
821 were obtained after unpaired t-test ($P(I_{2ctr})$ vs $P(I_2 | noI_1)$).

822

823 **Fig.5. Single cell vulnerability to *Salmonella* infection is a combination of intrinsic and**
824 **induced vulnerability. A.** The depicted cellular parameters were determined for HeLa cells
825 (upper panel) and Caco-2 cells (lower panel) as described in detail in *Materials and Methods*.
826 An overlay of the distribution of some of these parameters in infected (red) or non-infected
827 (blue) cells is shown. **B.** Quantification of the improvement of infection prediction by each cell
828 parameters by subtracting the likelihood (in log) of the model including all parameters from a
829 model ignoring one parameter. Results are averaged over 100 training/testing circles for
830 each model. P-values were obtained after paired t-test. **C.** Fold change of the probability of
831 infection as a function of the intrinsic vulnerability and of a previous infection. **D.** Increasing

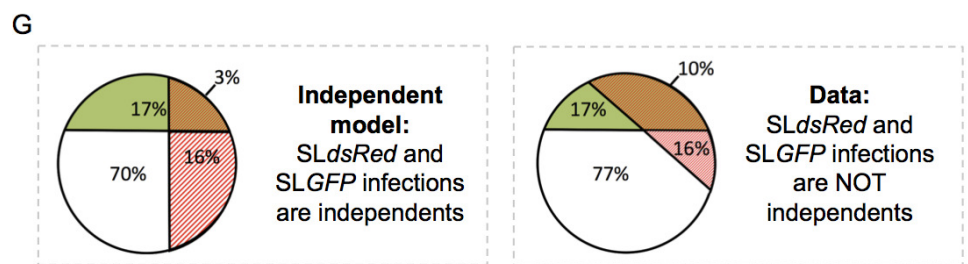
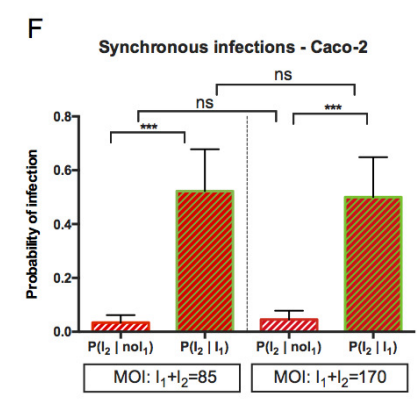
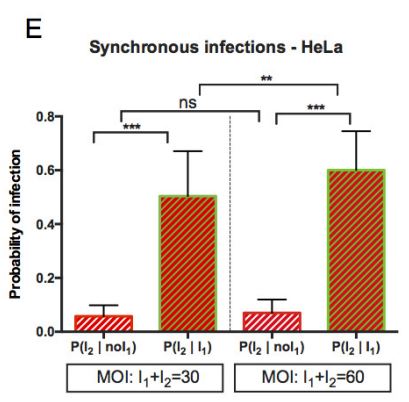
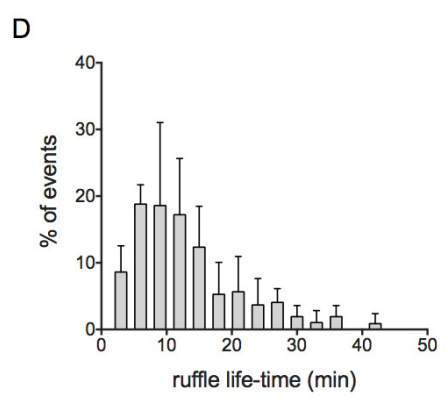
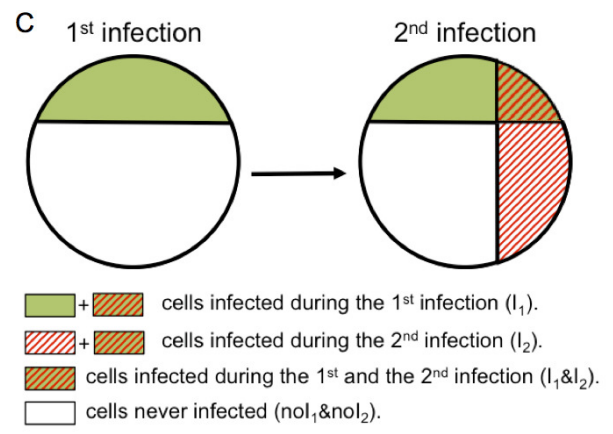
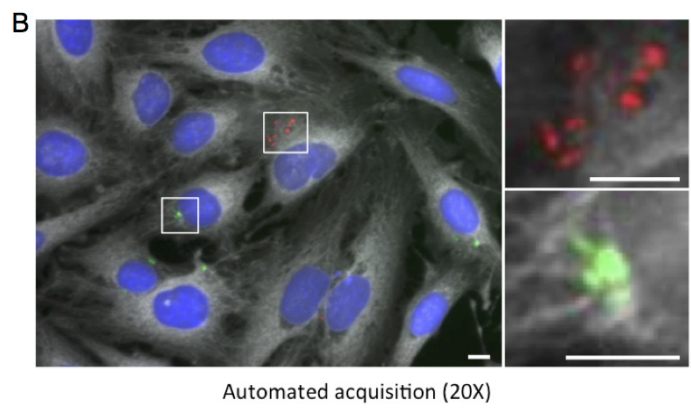
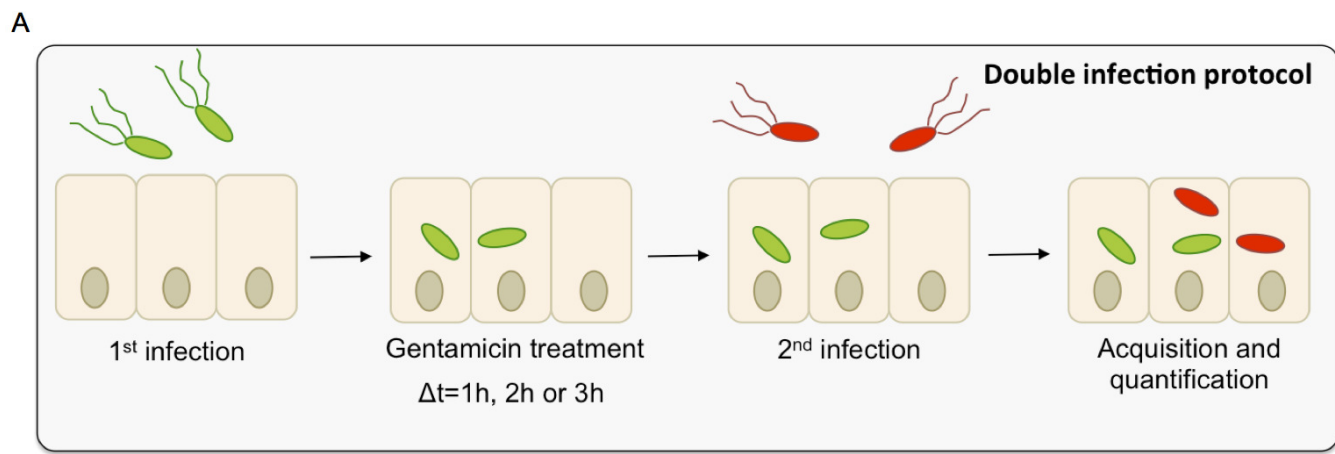
832 or decreasing of the probability of infection when the listed cell parameters increase their
833 values.

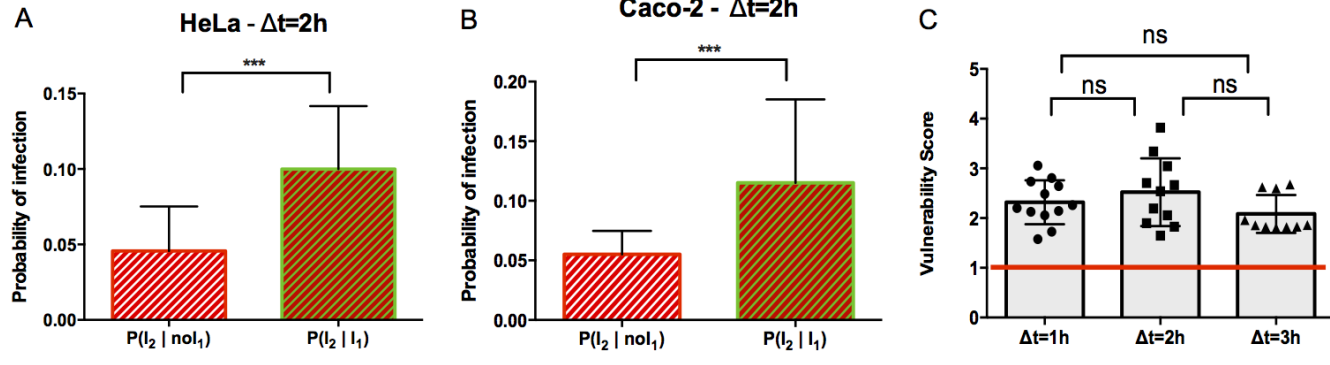
834

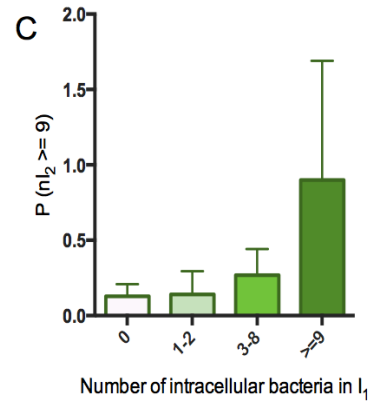
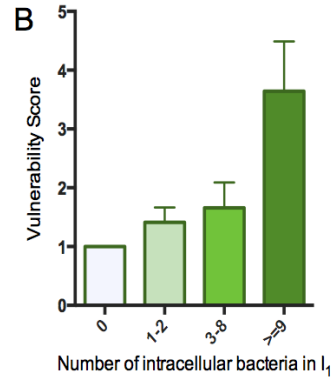
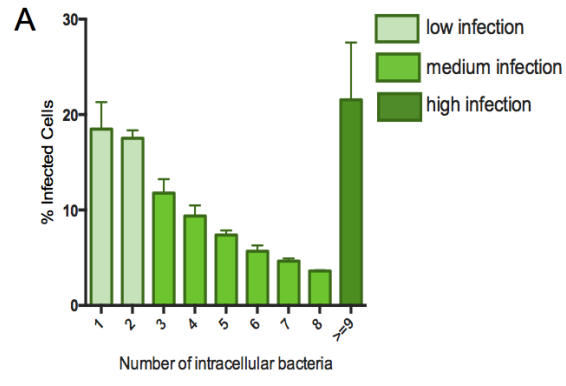
835 **Fig.6. Comparison of model-predicted vulnerability of single-cell with measured-**
836 **infection. A.** Model-predicted probability of infection displayed on reproduced original
837 images of HeLa cells (left panel). Colors are adapted for maximum contrast between lowest
838 (deep red) and highest (white) probability of infection. Measured infections from experiments
839 are shown (top-right panel). **B.** Estimation of the reliability of the two (HeLa and Caco-2)
840 models developed when tested on a total of 100 infected cells and 100 non-infected cells.

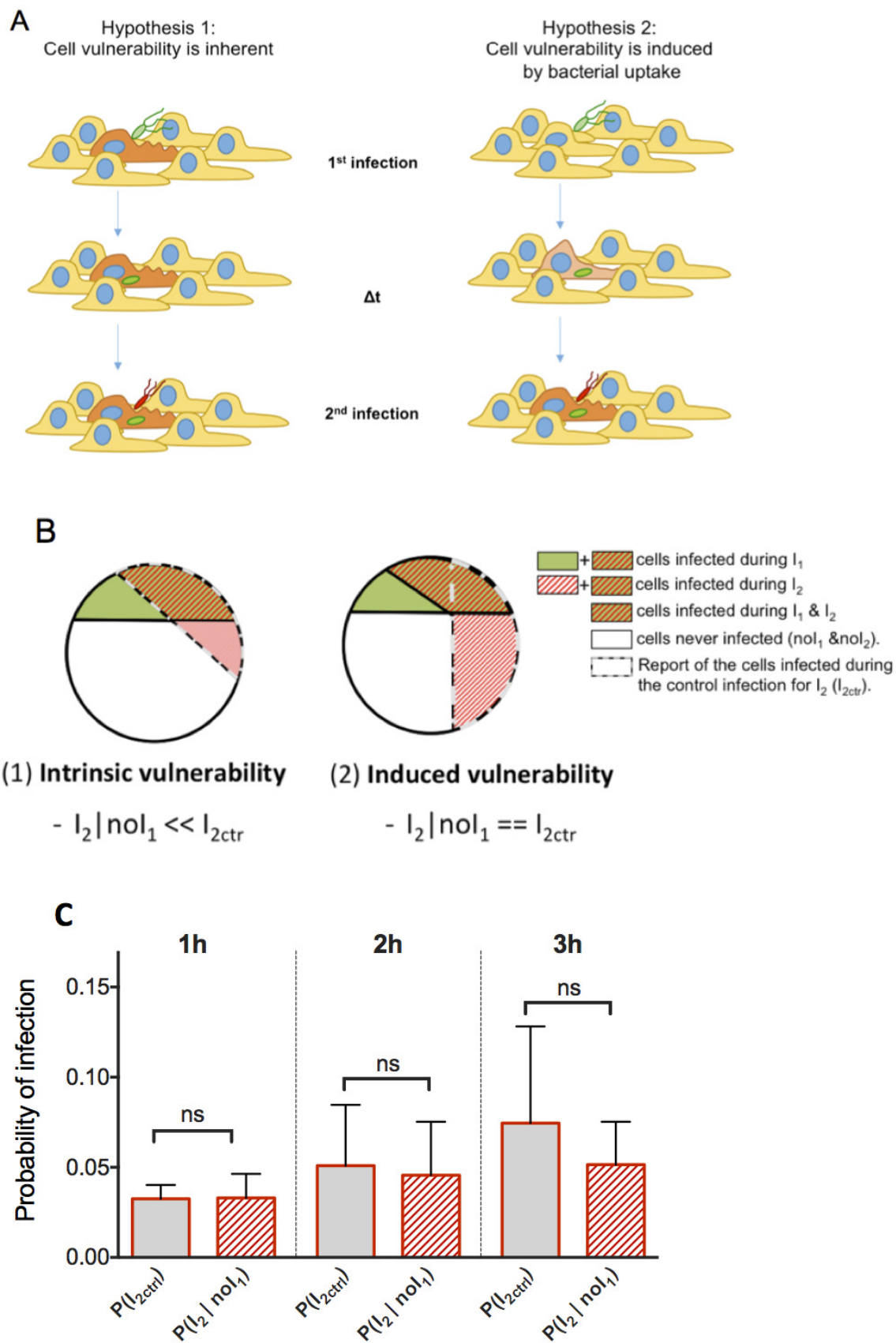
841

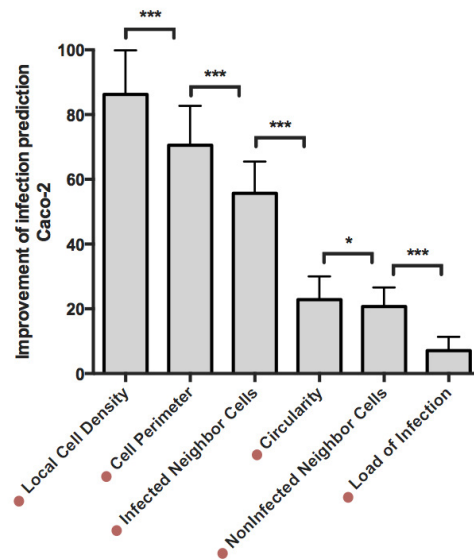
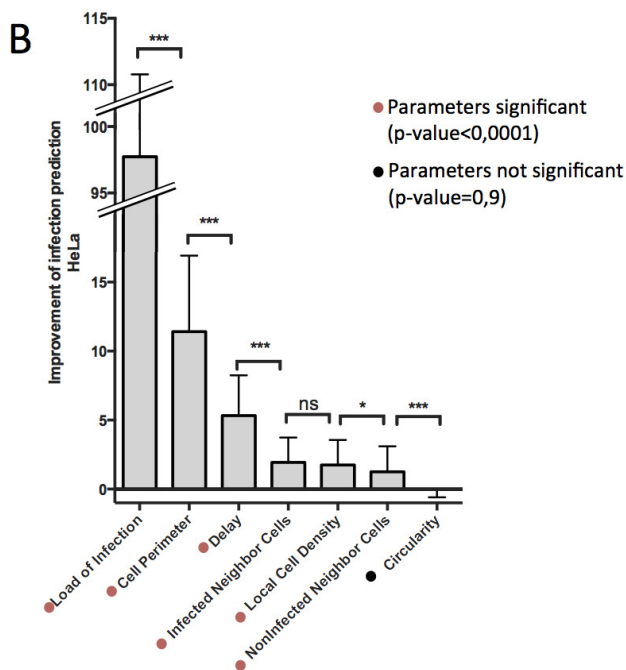
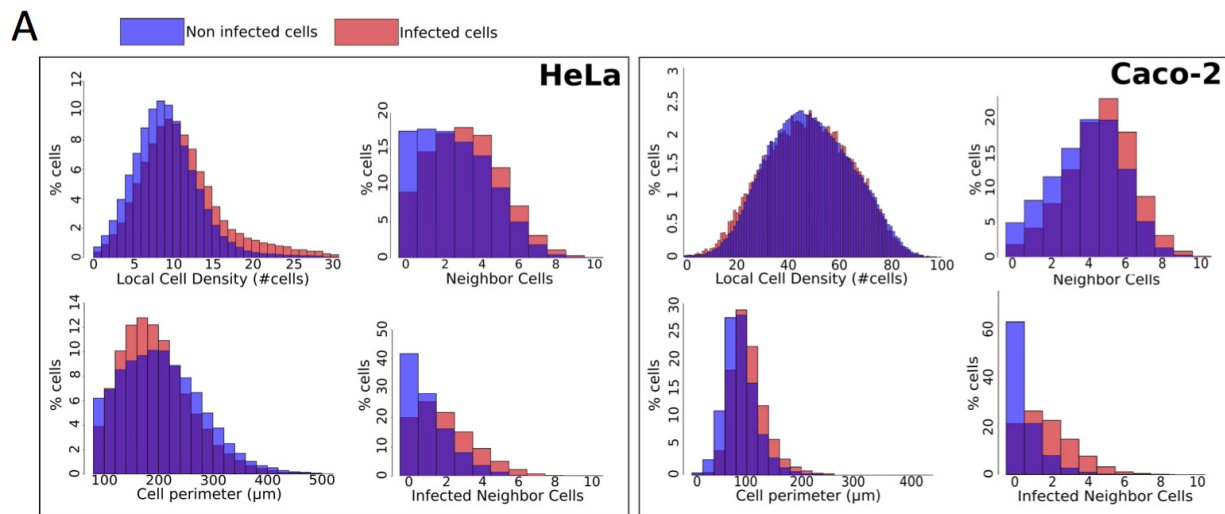
842 **Fig.7. Probability of infection as a function of single cell cholesterol level. A. B.**
843 Variation of the probability of *Salmonella* infection at different levels of host cholesterol
844 measured by FACS as described in detail in the text. Cholesterol levels were binned in five
845 categories at 20% steps from lowest to highest levels over the total cell population, each
846 category contains 20% of the whole cells. **A.** Results obtained for HeLa cells (n =3). **B.**
847 Results obtained for Caco-2 cells (n =3).











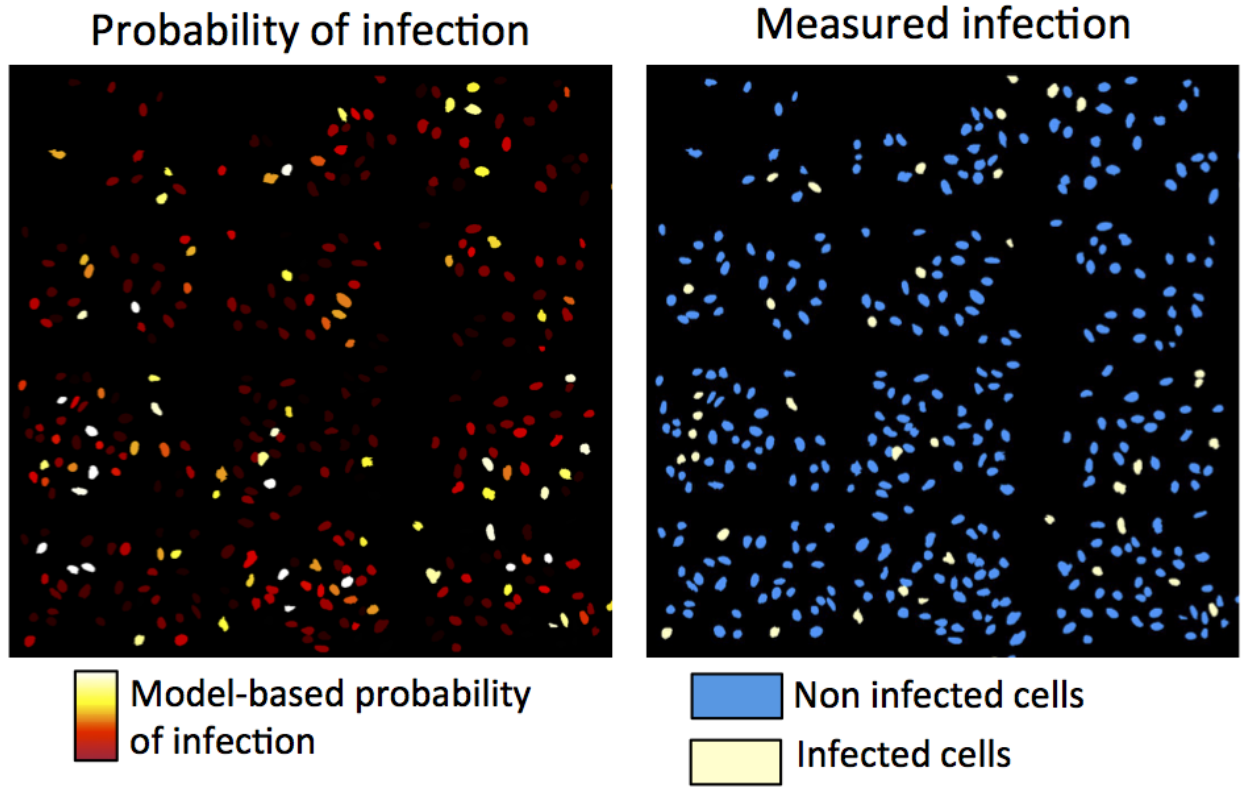
C Fold change of the probability of infection

Inherent vulnerability	1 st infection	HeLa	Caco-2
low	-	1	1
low	+	2.2	1.3
high	-	1.6	2.6
high	+	3.3	3.3

D Change in P(inf) when increase in the parameter values

Cell parameters	HeLa	Caco-2
Cell size	↗	↗
Circularity	≈	↘
Local cell density	↗	↘
Number of neighbor cells	↗	↗
Number of infected neighbor cells	↗	↗
Load of infection	↗	↗

A

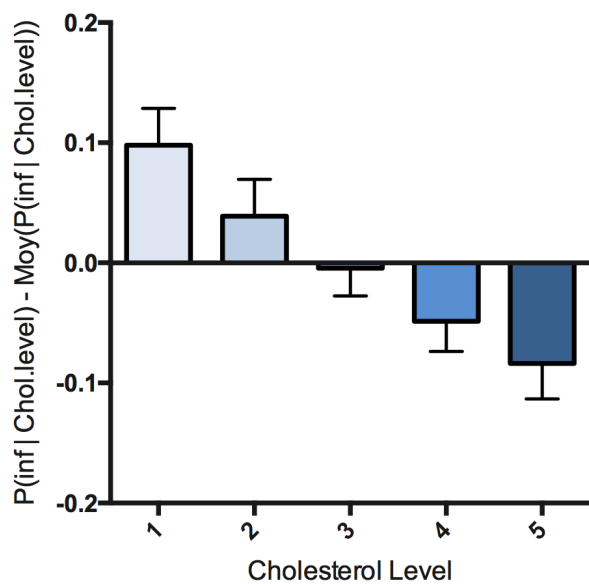


B

Model predictions	HeLa	Caco-2
True	62%	66%
False	38%	34%

A

P(inf | FilX) - HeLa



B

P(inf | FilX) - Caco-2

